Analysis of nonselective plasma etching of AlGaN by $CF_4/Ar/Cl_2$

V. Kuryatkov, B. Borisov, J. Saxena, S. A. Nikishin,[a] and H. Temkin
Department of Electrical Engineering, Texas Tech University, Lubbock, Texas 79409

S. Patibandla, L. Menon, and M. Holtz
Department of Physics, Texas Tech University, Lubbock, Texas 79409

(Received 19 October 2004; accepted 16 January 2005; published online 21 March 2005)

We report the nonselective plasma etching of epitaxial GaN:Mg, $Al_{0.63}Ga_{0.37}N$, and $AlN/Al_{0.08}Ga_{0.92}N$ short-period superlattices with various doping properties. Etching is performed using mixed CF_4/Ar feed gases in a combined inductively coupled plasma and reactive-ion etching chamber. A uniform etch rate of ~23 nm/min is obtained for each of the compositions studied under identical conditions. This nonselective etching is also found to preserve the surface uniformity studied by atomic force microscopy and quantified using surface roughness and lateral correlation length. By adding Cl_2 gas, etch rates are increased to 230–250 nm/min without degrading the surface properties. © *2005 American Institute of Physics*. [DOI: 10.1063/1.1866490]

I. INTRODUCTION

There has been substantial recent progress in the development of semiconductor-based optoelectronic devices, such as light-emitting diodes (LEDs) and solar blind photodetectors, which operate in deep ultraviolet (UV).[1–7] This progress stems from basic and applied research in growth, electrical and optical properties, and device processing. Currently, deep UV devices are based on AlGaN, for which the band gap spans 3.4–6.1 eV with increasing Al mole fraction. The devices are based on heterostructures and superlattices (SLs) of AlGaN materials with high AlN mole fraction.

A critical step in device experiments is plasma etching. Important etch characteristics are removal rate, anisotropy, and surface damage. Etching multiple compositions present in AlGaN heterostructures and SLs is challenging because the etch rate typically depends on Al content. For the generally used chlorine chemistry, GaN etches approximately three times faster than AlN.[8] An etch approach which is nonselective to Al composition would be advantageous from the simplicity, repeatability, and uniformity points of view. Furthermore, it has been observed that more aggressive etching elevates surface roughness.[8] This is particularly undesirable for contact formation, since oxides readily form on these surfaces and a rougher morphology serves to effectively thicken this layer. An additional issue in AlGaN etching is a delay in the onset of material removal, an effect which is generally attributed to the etch-resistant native oxide. The etch delay has recently been mitigated when etching AlN (Ref. 8) and AlGaN (Ref. 9) by using layers capped by GaN, which forms a less robust oxide. Han *et al.* examined a 70 -nm-thick $Al_{0.28}Ga_{0.72}N$ layer embedded in GaN (150-nm cap) etched using mixed $BCl_3/Ar/Cl_2$ gas.[9] They report etch rates ranging from 150 to 500 nm/min for both GaN and the alloy with plasma powers of 1000–2000 W. Exposed layers of AlGaN, with Al mole fraction as high as 35%, have been etched without delay using a BCl_3 breakthrough approach.[10] We find, however, few publications studying the efficacy of fluorine plasma chemistry on GaN etching[11] and none on AlGaN etching.

In this paper, we describe experiments on CF_4-based plasma etching of AlGaN layers with widely varying compositions. The etching is shown to be nonselective, to preserve surface roughness to <1 nm root-mean-square (rms) over 20×20 μm^2 areas, and to exhibit no etch delay. The absence of an etch delay is particularly significant, since the approach works even for layers with very high Al content and without the need for a GaN capping layer.[8,9] The addition of Cl_2 accelerates the etching by more than a factor of 10 without elevating the rms roughness. We organize the remainder of this paper to present experimental methods, followed by results demonstrating nonselective etching, studying the effects of varied etch parameters, and the measured surface properties. Finally, we summarize our findings.

II. EXPERIMENTAL METHODS

All layers used for our etching studies were grown using gas-source molecular-beam epitaxy. The different materials etched are listed in Table I. All SLs have an ~2 nm period and ~60% average Al composition. Details of the growth procedures can be found elsewhere.[1,2,12] All layers were grown on sapphire substrates and had a thickness of ~1 μm, with the exception of the 3-μm-thick $Al_{0.63}Ga_{0.37}N$ layer. All

TABLE I. List of layers used in this study.

Layer	Doping
$AlN/Al_{0.08}Ga_{0.92}N$ SL	Mg
$AlN/Al_{0.08}Ga_{0.92}N$ SL	none
$AlN/Al_{0.08}Ga_{0.92}N$ SL	Mg
GaN	Mg
$Al_{0.63}Ga_{0.37}N$	none
$AlN/Al_{0.08}Ga_{0.92}N$ SL	Si/Mg junction

[a]Electronic mail: sergey.nikishin@coe.ttu.edu

TABLE II. Basic etching parameters.

Plasma parameter	Value
Chamber pressure	10 mTorr
ICP power	300 W
RIE power	150 W
CF_4/Ar flow rates	20/4 SCCM

the materials have been characterized using x-ray diffraction, cathodoluminescence, and optical reflectance to verify their structural and optical quality.[13–15]

The etching was conducted in a commercial inductively coupled plasma (ICP) reactive-ion etching (RIE) system, which has been described elsewhere.[8] The etching was investigated as a function of ICP power, RIE power, CF_4/Ar gas composition, and chamber pressure. The basic etching conditions are summarized in Table II. Holding the other parameters fixed, we systematically varied each parameter in turn to study its role in the etching. For elevated etch rates, Cl_2 was added to the mixture and its effect on etch rate and roughness were likewise studied. The etch step height was determined using a stylus profilometer. Surface properties were studied using atomic force microscopy (AFM) operated in the noncontact mode. We rely here on "large" area images, 20×20 μm^2, analyzing the rms surface roughness (σ),

$$\sigma^2 = \frac{\sum_{i,j=1}^{N,M} (h_{i,j} - \bar{h})^2}{(N-1)(M-1)}, \tag{1}$$

where $h_{i,j}$ is the height at $\mathbf{r}=(x,y)$ coordinate, denoted as (i,j), $N\times M$ is the total number of points constituting the image, and $\bar{h}$ is the average surface height. For our starting material, we observe a rms roughness of ~0.80 nm, which is exceptionally smooth. In addition to roughness, we also examine the height correlation function,

$$G(\rho,t) = \langle [h(\mathbf{r}_1,t) - h(\mathbf{r}_2,t)]^2 \rangle, \tag{2}$$

with $\rho=|\mathbf{r}_2-\mathbf{r}_1|$ to obtain both the scaling exponent α in $G(\rho,t)\sim\rho^{\alpha}$ and the cutoff length L_c, which corresponds to the typical fine-scale feature sizes seen in our AFM images.

III. NONSELECTIVE ETCHING

Figure 1 summarizes the etch depth with process duration using the basic conditions in Table II. Under these conditions the etch rate is 23 ± 2 nm/min for each of the cases studied (Table I). For comparison, Cl_2/Ar plasma etches GaN much faster, at a rate of 600 nm/min under identical conditions.[8] Previous results, obtained under similar chlorine etching conditions, report GaN removal rates of ~40 nm/min (Ref. 16) to 250 nm/min.[17] The addition of BCl_3 to the process accelerates this etching.[9,18] AlN etches significantly slower with Cl_2/Ar plasma. For example, Ref. 8 reports AlN to etch at ~170 nm/min with the same recipe that etches GaN at 600 nm/min. The ~23-nm/min etch rate of the AlGaN alloy layer and the AlN/AlGaN short-period SLs are also quite slow. For comparison, similar SLs were found to etch at approximately 200 nm/min using a similar

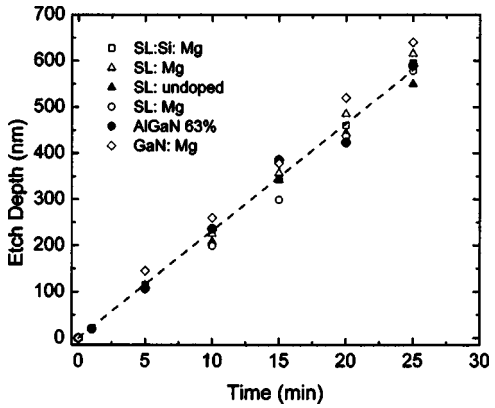

FIG. 1. Etch depth vs process time for the samples listed in Table I.

Cl_2/Ar approach.[19] The noted advantage of our current result is that the etch rate, albeit slow, is independent of the specific composition of the AlGaN being etched.

A second distinct advantage to our CF_4/Ar method is the absence of an etch delay. This is particularly important in the Al-rich alloys and SLs, where chemically robust native oxides can form. The delay seen in the onset of etching has been attributed to this oxide formation.[19] The delay can be in excess of 90 s in $Al_{0.35}Ga_{0.65}N$, although a 60-s BCl_3 pretreatment rapidly breaks through the oxide with a subsequent etch rate of ~10 nm/min in Cl_2.[10] In our experiments we have intentionally avoided the use of BCl_3, in favor of the less aggressive CF_4. It is well known that carbon fluoride compounds are effective at etching SiO_2 because oxygen is readily scavenged from the surfaces and plasma through the formation of COF_2, CO, and CO_2.[20] We suggest that in the etching of Al-rich AlGaN, the CF_4-related species serve a similar function, thereby helping cut through the initial native oxide layer by removing oxygen from the surface and minimizing reattachment from the plasma to the surface by binding it into nonreactive compounds. As discussed in Sec. IV, we also consider physical etching to play an important role. Physical etching will be less discriminatory in the surface stoichiometry it attacks.

We have established that our etching procedure is nonselective and does not exhibit a significant etch delay. We now focus on the AlGaN layer with an AlN mole fraction of 63%. This material has an optical band gap of 4.77 eV (260 nm), representative of the AlN content important to deep UV devices. It is also in a content range that is representative of state-of-the-art wide-band-gap materials, including the short-period SLs examined in Table I and Fig. 1.

IV. EFFECTS OF PLASMA PARAMETERS ON ETCHING ALGAN

Figure 2 summarizes the dependence of etch rate on plasma parameters for the $Al_{0.63}Ga_{0.37}N$ material. Also shown are the rms roughness results, which will be discussed in Sec. V. In Fig. 2(a) we exhibit the etch rate dependence on CF_4 flow rate (Φ) expressed as a percent fraction, $100\times\Phi(CF_4)/[\Phi(CF_4)+\Phi(Ar)]$. A higher CF_4 flow will enhance the chemical component of etching, although a high CF_4 content, at the expense of Ar, has a propensity to pro-

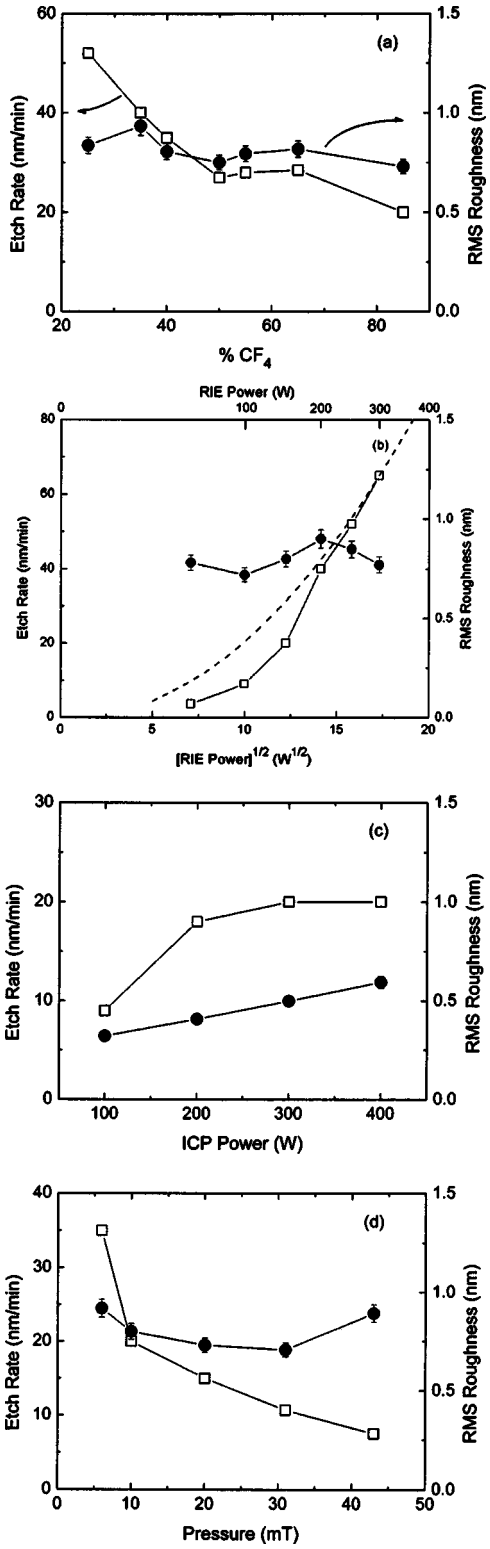

FIG. 2. Summary of etch rate (open squares) vs varied individual plasma parameters: (a) percent CF_4 flow, (b) RIE power (note the square root), (c) ICP power, and (d) chamber pressure, holding other parameters at the basic conditions listed in Table II. The right-hand scale is the rms roughness (filled circles) obtained from 20×20 μm^2 AFM scan areas. In (b) we also show the calculated Bohm flux dependence on RIE power.

duce protective polymers.[21] Starving the process of Ar diminishes the efficiency at which these polymers are physically removed from the surface, which has the effect of exposing fresh material to be etched. Argon is also used to increase the plasma density and elevate the radical formation through dissociation of the CF_4. This process thereby increases the fluorine to CF_x ratio, which is known to improve chemical etching.[21] In the low flow-rate range, we expect the physical removal of the material to play a role as energetic argon ions sputter the surface. The overall trend seen in Fig. 2(a) is a slightly diminishing etch rate with increasing CF_4 flow. This suggests that the two removal processes, physical and chemical, are both important in etching AlGaN. The conclusion that physical and chemical etching are important is also consistent with the nonselective nature of our etch.

Figure 2(b) shows the dependence of etch rate on RIE power. The etch rate is slow to $\sim$100 W before increasing rapidly. This suggests a minimum RIE power requirement below which etching is negligible. Using the standard approach of plotting the etch rate versus the square root of power we find the etch rate to increase above a power of 84 ± 8 W, indicating that this power is required for the onset of etching. Also shown in Fig. 2(b) is the calculated Bohm flux[22] of ions at the target surface as a function of the RIE power. Primary input parameters in this calculation include susceptor area, gas pressure (through the plasma density and electron Debye wavelength), and input power. Secondary factors, which were found to have little influence on the curve, were electron temperature and collisional electron energy loss. This flux is related, in the current context, to bombardment at the etching surface, i.e., the physical component of etching. The flux exhibits a gradual increase at low RIE power, followed by a more substantial rise beginning near 100 W. (The ion density exhibits a similar dependence.) This dependence is in reasonable agreement with the measured etch rates, suggesting that the physical etch mechanism is important for the etch conditions used here. Figure 2(c) shows the etch rate to rise with ICP power below 200 W, then to saturate at $\sim$20 nm/min. The rise in etch rate is attributed to the increase in density of etching species with ICP power. For the basic conditions used, this factor appears to reach an optimum near 200 W, above which solely increasing the ICP power does not raise the plasma density. In Fig. 2(d) we show the etch rate dependence on chamber pressure. The etch rate is seen to drop dramatically with pressure, an effect we attribute to the $\sim$ one order of magnitude decrease in the particle mean free path. This is commensurate with the important role surface bombardment plays in this etching.

We also experimented with adding Cl_2 to the etching chemistry in order to obtain faster etch rates. Figure 3 shows etch rate (and rms roughness) versus Cl_2 percentage according to $100\times\Phi(Cl_2)/[\Phi(Cl_2)+\Phi(CF_4)]$, with a fixed Ar flow rate $\Phi(Ar)=4$ SCCM (denotes cubic centimeter per minute at STP). The etching occurs at a very high rate, when compared with all the etch rates in Fig. 2. Using this approach, the etch rate is readily varied by a factor of $\sim$10 with the added flow of the Cl_2 gas. Clearly, plasma etching by chlorine chemistry is highly advantageous. We discuss the roughness factors Sec. V.

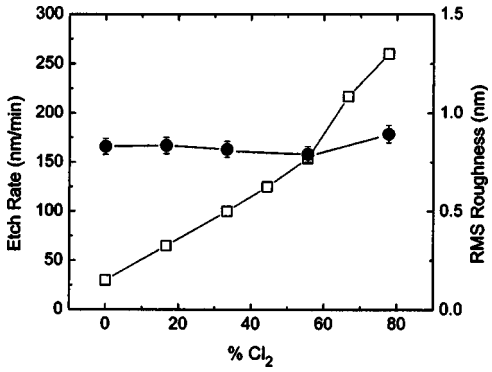

FIG. 3. Etch rate (open squares) vs percent Cl_2 in CF_4/Ar. The other conditions are as in Table I. The right-hand scale is the rms roughness (filled circles) from 20×20 μm^2 AFM scan areas.

V. EFFECTS OF ETCHING ON SURFACE PROPERTIES

A typical AFM image of AlGaN, obtained following etching for 60 s, is shown in Fig. 4(a) (20×20 μm^2 scan). Clearly seen is a grainy appearance. A more detailed 1×1 μm^2 image is shown in Fig. 4(b). The grains are seen with a reproducible lateral size of 300–400 nm. We attribute these features to columnar domains typical of epitaxial III nitrides. The fact that we observe these features following etching implies that the surfaces are preserved.

The image in Fig. 4(a) is determined to have a rms roughness of 0.82 nm. Similar analyses are carried out for each postetch sample. Included in each panel of Figs. 2 and 3 are the rms roughness values obtained from postetch AFM images. Prior to etching, the rms roughness of the AlGaN was 0.80 nm. The postetch rms roughness values are uniformly below 1.0 nm, quantitatively demonstrating that all the etching procedures preserve the smooth growth surfaces. This result extends to the more aggressive Cl_2 etching. It was reported in Ref. 8 that surfaces roughen significantly when etching either GaN or AlN above critical etch rates of 400 and 90 nm/min, respectively. The fastest etch rate achieved in the current work is ~260 nm/min. Since AlGaN layers were not investigated in the prior work, an analogous value has not been established. Assuming that the alloy will exhibit a critical etch rate, for the onset of roughening, which lies between that of GaN and AlN, it is possible that our maximum etch rate here has not exceeded that value. It is also possible that the presence of CF_4 in the etching chemistry mitigates the roughening processes by minimizing the formation of stable oxides, as discussed in Sec. III. Further experiments are needed to elucidate the role of CF_4 in surface roughening.

We have also analyzed the rms roughness on smaller area (1×1 μm^2) AFM images. The roughness values obtained from these images are, in general, slightly lower than those from the larger images, suggesting a scaling dependence. To check this, we calculated the height correlation functions for each AFM image using Eq. (2). An example is shown in Fig. 5 for the AFM image of Fig. 4(a). The length range shown is restricted to lie between the AFM tip diameter and ~1/5 the image size. The dependence shows scaling below a cutoff length of $L_c \sim 400$ nm. This characteristic length is in approximate agreement with the fine-scale features seen in Figs. 4(a) and 4(b). Scaling is absent above L_c because there is little contribution to the roughness above this length scale. Below L_c, scaling is present due to the fine-scale roughness present on the surface. The scaling coefficient in Fig. 5 is $\alpha = 0.81 \pm 0.02$. In all cases studied here, the scaling coefficient is between 0.73 and 0.86. This value is consistent with what has been reported in previous etch studies,[8,23,24] and is commensurate with little contribution to roughening from local geometrical features[25] such as topographical variations in the surface. In addition, the value of L_c ranges between 320 and 480 nm for all etching experiments carried out here. AFM measurements of the as-grown surfaces reveal a similar variation in cutoff length. The small

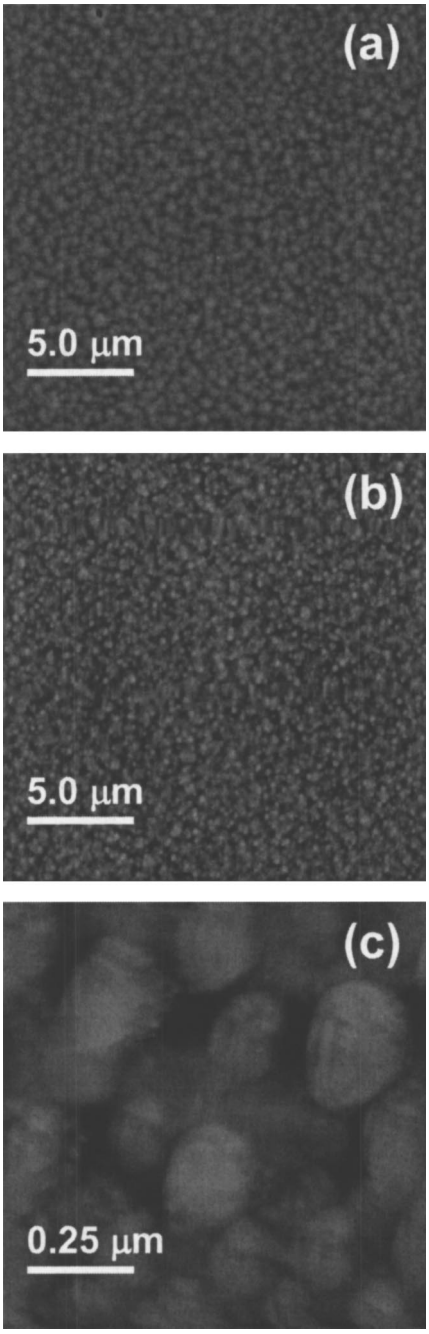

FIG. 4. AFM images of $Al_{0.63}Ga_{0.37}N$ following a 60-s etch with 150 W RIE power, 300 W ICP power, 10 mTorr chamber pressure, and CF_4/Ar feed gas: (a) 20×20 μm^2 scan area and (b) 1×1 μm^2 scan area.

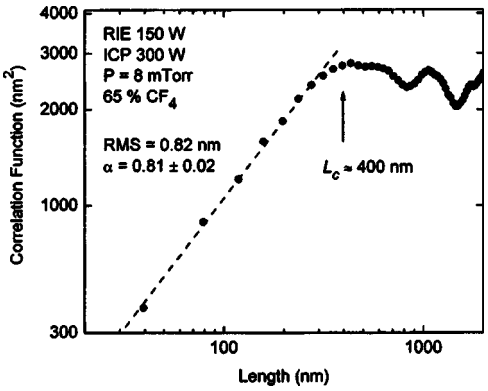

FIG. 5. Correlation length analysis of the AFM data shown in Fig. 4(a).

variation corroborates the conclusion that surface smoothness is preserved by the etching described in this paper.

VI. SUMMARY

We have used CF_4/Ar to plasma etch an $Al_{0.63}Ga_{0.37}N$ alloy, along with GaN and SLs composed of $AlN/Al_{0.08}Ga_{0.92}N$. As seen in Fig. 1, etching is nonselective across this composition list, and is accompanied by no etch delay. These attributes make this method highly desirable for processing experiments on devices with varied compositions, such as heterostructures and SLs. Additionally, the etching preserves well the initially smooth surfaces of the as-grown materials, as shown in Fig. 2. With CF_4 and Ar as the only feed gases, the etch rates are very slow, below 60 nm/min. However, the addition of Cl_2 to the CF_4/Ar mixture can be used to adjust the etch rate to ~260 nm/min (at the maximum Cl_2 flow rate attempted) without inducing further roughness (Fig. 3). Detailed surface analysis, using the height correlation function, further supports the consistently smooth surface morphology produced by this plasma etch.

The authors acknowledge support from the National Science Foundation (Grant Nos. ECS-0323640 and ECS-0304224), DARPA (Dr. J. Carrano), U.S. Army SBCCOM, NATO Science for Peace (974505), and the J. E. Maddox Foundation.

[1] G. Kipshidze, V. Kuryatkov, B. Borisov, S. A. Nikishin, M. Holtz, S. N. G. Chu, and H. Temkin, Phys. Status Solidi A **192**, 286 (2002).
[2] S. A. Nikishin, V. Kuryatkov, A. Chandolu, B. Borisov, G. Kipshidze, H. Temkin, I. Ahmad, and M. Holtz, Jpn. J. Appl. Phys., Part 2 **42**, L1362 (2003).
[3] A. Yasan, R. McClintock, K. Mayes, D. Shiell, L. Gautero, S. R. Darvish, P. Kung, and M. Razeghi, Appl. Phys. Lett. **83**, 4701 (2003).
[4] A. Hanlon, P. M. Pattison, J. F. Kaeding, R. Sharma, P. Fini, and S. Nakamura, Jpn. J. Appl. Phys., Part 2 **42**, L628 (2003).
[5] A. J. Fischer *et al.*, Appl. Phys. Lett. **84**, 3394 (2004).
[6] V. Adivarahan, S. Wu, J. P. Zhang, A. Chitnis, M. Shatalov, V. Mandavilli, R. Gaska, and M. A. Khan, Appl. Phys. Lett. **84**, 4762 (2004).
[7] H. Temkin, in *Advanced Semiconductors and Organic Nano-Techniques*, edited by H. Morkoc (Academic, New York, 2003), Vol. III.
[8] K. Zhu *et al.*, J. Appl. Phys. **95**, 4635 (2004).
[9] Y. Han, S. Xue, T. Wu, Z. Wu, W. Guo, Y. Luo, Z. Hao, and C. Sun, J. Vac. Sci. Technol. A **22**, 407 (2004).
[10] D. Buttari *et al.*, Appl. Phys. Lett. **83**, 4779 (2003).
[11] M. Wintrebert-Fouquet, K. S. A. Butcher, and S. K. H. Lam, *Comparisons of Gallium Nitride and Indium Nitride Properties After CF4/Argon Reactive Ion Etching*, MRS Symposia Proceedings No. 743 (Materials Research Society, Pittsburgh, 2003), p. L3.55.1.
[12] S. Nikishin, N. N. Faleev, A. S. Zubrilov, V. G. Antipov, and H. Temkin, J. Appl. Phys. **76**, 2910 (2000).
[13] V. Kuryatkov, A. Chandolu, B. Borisov, G. Kipshidze, K. Zhu, S. A. Nikishin, H. Temkin, and M. Holtz, Appl. Phys. Lett. **82**, 1323 (2003).
[14] V. Kuryatkov *et al.*, Appl. Phys. Lett. **83**, 1319 (2003).
[15] M. Holtz *et al.*, J. Appl. Phys. **89**, 7977 (2001).
[16] Y. B. Hahn *et al.*, J. Vac. Sci. Technol. A **17**, 768 (1999).
[17] J. W. Lee *et al.*, J. Vac. Sci. Technol. B **14**, 3637 (1996).
[18] S. Tripathy, A. Ramam, S. J. Chua, J. S. Pan, and A. Huan, J. Vac. Sci. Technol. A **19**, 2522 (2001).
[19] K. Zhu, V. Kuryatkov, B. Borisov, G. Kipshidze, S. A. Nikishin, H. Temkin, and M. Holtz, Appl. Phys. Lett. **81**, 4688 (2002).
[20] C. J. Mogab, A. C. Adams, and D. L. Flamm, J. Appl. Phys. **49**, 3796 (1978).
[21] J. W. Coburn and H. F. Winters, J. Vac. Sci. Technol. **16**, 391 (1979).
[22] M. A. Lieberman and A. J. Lichtenberg, *Principles of Plasma Discharges and Materials Processing* (Wiley, New York, 1994).
[23] S. W. Robey, Phys. Rev. B **65**, 115306 (2002).
[24] J. H. Schmid, A. Ballestad, B. J. Ruck, M. Adamcyk, and T. Tiedje, Phys. Rev. B **65**, 155315 (2002).
[25] M. Kardar, G. Parisi, and Y.-C. Zhang, Phys. Rev. Lett. **56**, 889 (1986).